

CarbonBench: A Global Benchmark for Upscaling of Carbon Fluxes Using Zero-Shot Learning

Aleksei Rozanov
rozan012@umn.edu
University of Minnesota
Minneapolis, MN, USA

Yimeng Zhang
zhan8460@umn.edu
University of Minnesota
Minneapolis, MN, USA

Arvind Renganathan
renga@umn.edu
University of Minnesota
Minneapolis, MN, USA

Vipin Kumar
kumar001@umn.edu
University of Minnesota
Minneapolis, MN, USA

Abstract

Accurately quantifying terrestrial carbon exchange is essential for climate policy and carbon accounting, yet models must generalize to ecosystems underrepresented in sparse eddy covariance observations. Despite this challenge being a natural instance of zero-shot spatial transfer learning for time series regression, no standardized benchmark exists to rigorously evaluate model performance across geographically distinct locations with different climate regimes and vegetation types.

We introduce *CarbonBench*, the first benchmark for zero-shot spatial transfer in carbon flux upscaling. *CarbonBench* comprises over 1.3 million daily observations from 567 flux tower sites globally (2000–2024). It provides: (1) stratified evaluation protocols that explicitly test generalization across unseen vegetation types and climate regimes, separating spatial transfer from temporal autocorrelation; (2) a harmonized set of remote sensing and meteorological features to enable flexible architecture design; and (3) baselines ranging from tree-based methods to domain-generalization architectures. By bridging machine learning methodologies and Earth system science, *CarbonBench* aims to enable systematic comparison of transfer learning methods, serves as a testbed for regression under distribution shift, and contributes to the next-generation climate modeling efforts.

Keywords

Transfer learning, zero-shot learning, domain generalization, benchmark, upscaling, carbon fluxes

1 Introduction

As highlighted by the 2023 Intergovernmental Panel on Climate Change (IPCC) assessment [23], anthropogenic CO₂ emissions have unequivocally driven global temperature increases across atmosphere, land, and ocean. While numerous carbon removal approaches are under development [1, 12, 40], biological sequestration, i.e. the photosynthetic capture and storage of CO₂ as biomass and soil organic carbon, remains one of the few scalable natural mechanisms for atmospheric decarbonization.

Eddy covariance (EC) [3] towers provide an on-ground instrumented way to quantify this process through measuring net

ecosystem exchange (NEE), representing land–atmosphere carbon flux within a footprint extending up to roughly 3,000 m around the tower [7]. Despite their widespread use, eddy covariance (EC) observations remain geographically sparse due to high operational costs, technical complexity, and inaccessibility of certain regions (e.g., tropical rainforests or high-latitude ecosystems). Furthermore, EC data is publicly available only from < 700 sites, with a combined spatial footprint of flux towers at less than 0.015% of the Earth’s terrestrial surface. While EC measurements provide high-fidelity flux estimates at individual sites, this coverage is insufficient to produce spatially continuous assessments of global carbon sequestration needed for climate policy, carbon accounting, and the calibration and validation of Earth system models (e.g., CESM, CMIP).

Researchers have therefore developed regional and global-scale datasets by posing the **upscaling** problem [13], i.e., a *bottom-up* task that infers continuous flux fields from point-level EC observations using gridded covariate data. Several global products including FLUXCOM [17, 26] and MetaFlux [25] have been produced using mostly classical ML approaches such as gradient boosting and ensemble methods, with growing interest in deep learning and transfer learning approaches.

From a machine learning perspective, this setting naturally corresponds to a **zero-shot spatial transfer learning problem**, where models must generalize to geographically distinct locations with no prior observations. Each geographical location represents a distinct domain with its own climate regime, vegetation type, and environmental characteristics, making this a natural instance of domain generalization. The model must learn mappings from meteorological and remote sensing features, along with site-specific metadata such as vegetation type and climate class, to predict carbon fluxes at entirely new locations without any labeled flux data.

However, carbon flux upscaling remains particularly challenging due to strong spatial heterogeneity, non-uniform data availability and quality. Flux–feature relationships are highly context-dependent; e.g., the same satellite-derived vegetation index and meteorological conditions may indicate different carbon flux values at different locations. As a result, models trained on well-observed locations often perform well in-distribution but degrade sharply when applied to new geographical regions. Compounding this challenge, observational coverage is most

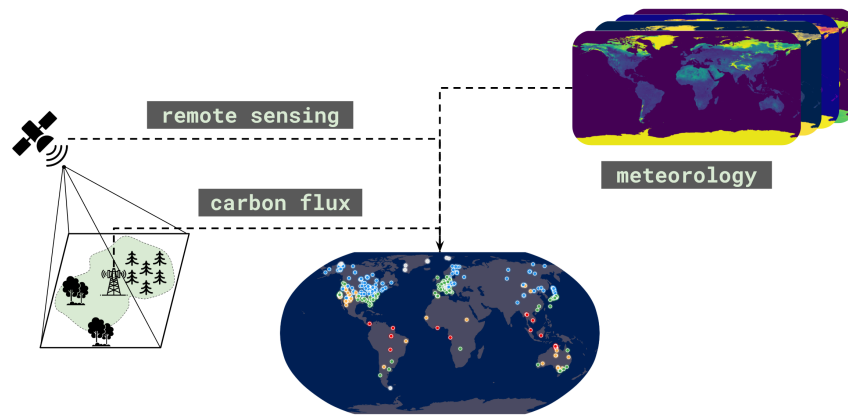


Figure 1: Overview of the *CarbonBench* setup. Eddy covariance flux observations provide sparse footprint-level targets, while remote sensing and meteorological data serve as gridded inputs for spatial generalization.

sparse in regions critical to the global carbon cycle: 1) tropical ecosystems (high productivity, year-round growing seasons that disproportionately contributing to the carbon exchange) and 2) high-latitude regions (that are undergoing rapid warming and permafrost thaw leading to critical shifts in the global carbon cycle). Robust spatial transfer learning is therefore essential for global-scale flux estimation.

There is a growing interest in both ML and domain science communities in taking advantage of advances in machine learning, many of which have been developed in related contexts across entirely different problem domains. As an example, recent works have increasingly emphasized domain generalization and task-aware learning strategies that aim to separate location-specific variability from shared ecosystem dynamics [25, 36]. However, progress in carbon flux upscaling remains constrained by methodological gaps on the machine learning side:

Gap I. Transfer learning for time series regression remains underrepresented in the ML research landscape. Unlike classification, **regression under distribution shift** is dominated by systematic errors rather than discrete misclassifications: shifts in scale, variance, or noise structure across domains can lead to biased predictions even when inputs appear similar. Continuous domain heterogeneity further alters input–target relationships, making distribution shift difficult to detect and correct. Addressing these challenges requires: (1) absolute and scale-normalized metrics to detect magnitude-dependent biases, (2) stratified evaluation to prevent performance in dominant domains from masking failures in underrepresented regions, and (3) baselines suited to continuous targets rather than classification. No existing standardized evaluation framework for time series or classification-oriented transfer learning provides this combination.

Gap II. Most existing frameworks for time series regression and forecast primarily assess temporal generalization (i.e., temporal extrapolation) at fixed locations (e.g., Monash Archive, Informer benchmarks). They do not address spatial generalization across geographically distinct locations with different environmental contexts, despite this being the natural problem structure for carbon flux upscaling and many other scientific applications. This limitation is particularly critical for carbon flux upscaling, where the most important biomes (tropical, high-latitude) are precisely

those with weakest observational coverage. Addressing this gap requires: (a) stratified evaluation across climate zones and vegetation types, and (b) standardized protocols for comparing domain generalization and transfer learning architectures.

Gap III. Carbon flux upscaling has remained largely isolated from mainstream machine learning research, limiting the adoption of recent advances in representation learning, transfer learning, and generalization. At the same time, spatial transfer learning for time series regression remains largely underexplored within the ML community, despite rapid progress in domain generalization and adaptation methods. This disconnect has slowed cross-pollination between the two fields, leaving a clear opportunity to align scientifically meaningful problems with active ML research directions.

There is increasing interest in both ML and domain science communities in addressing these challenges, many of which have been researched in related contexts across entirely different problem domains. However, these gaps (domain and ML) make meaningful comparison across methods for carbon upscaling difficult. Existing studies differ substantially in their choice of flux tower sites, input features, target variables, and evaluation approaches, making the reported improvements difficult to reproduce, compare, and interpret.

To address these challenges, we introduce *CarbonBench*, the first comprehensive transfer learning benchmark for upscaling terrestrial CO_2 fluxes that simultaneously advances both scientific modeling of carbon flux cycles and methodological development of spatial transfer learning for time series regression (which can be seen as a domain generalization or adaptation problem). This benchmark makes systematic comparison easier and allows the community to experiment with existing transfer learning approaches tried in other domains. *CarbonBench*¹ enables systematic evaluation and comparison of diverse model architectures under zero-shot spatial generalization settings and comprises the following components:

- A harmonized set of meteorological and remote sensing features at daily temporal resolution for each flux tower site (enables standardized comparison across studies);

¹Code:<https://github.com/alexrxro/CarbonBench>

- A dedicated Python library for building highly customizable workflows, supporting data analysis, feature engineering and selection, efficient data loading, model training using *PyTorch* [30], and standardized evaluation (Problem III: ML/carbon flux disconnect);
- Benchmarked state-of-the-art machine learning models – including tree-based methods, recurrent architectures, transformers, and meta-learning approaches – evaluated using regression-appropriate metrics (R^2 , RMSE, normalized MAE) under a rigorous zero-shot evaluation protocol, establishing baseline performance for future comparisons (Problems I and III: benchmarking time series regression under transfer learning setting and cross-pollination);
- Two comprehensive train–test splits stratified by both climate and vegetation type to expose scale-dependent biases across domains and comprehensively assess global model generalization (Problem II: spatial generalization).

More importantly, *CarbonBench* enables investigation of previously underexplored questions about spatial transfer learning for carbon flux upscaling:

- (1) How do different neural architectures handle distribution shifts in time series regression?
- (2) Do models explicitly designed for transfer learning exhibit better spatial generalization than standard supervised approaches?
- (3) Can domain generalization and adaptation architectures be successfully used in the zero-shot spatial transfer learning setting?
- (4) Which meta-learning strategies are most effective for spatial adaptation?
- (5) Can models learn ecosystem dynamics that generalize across geographical regions, and does this improve performance in poorly observed biomes?

2 Problem Formulation

2.1 Carbon Flux Upscaling as Spatial Regression

Let $\Omega \subset \mathbb{R}^2$ denote the spatial domain (e.g., the Earth’s land surface) and let $\mathcal{T} = \{1, 2, \dots, T\}$ represent the temporal domain with daily resolution. We are given a set of eddy covariance tower observations:

$$\mathcal{D} = \{(s_i, \mathbf{z}_i, \mathbf{x}_{i,t}, \mathbf{y}_{i,t}, t) \mid i = 1, \dots, N; t \in \mathcal{T}_i\} \quad (1)$$

where:

- $s_i = (\text{lat}_i, \text{lon}_i) \in \Omega$ denotes the spatial coordinates of site i ;
- \mathbf{z}_i represents site-specific metadata (IGBP vegetation type, Köppen climate class);
- $\mathbf{x}_{i,t} \in \mathbb{R}^F$ is the feature vector (drivers) at site i and time t , comprising:

$$\mathbf{x}_{i,t} = [\mathbf{x}_{i,t}^{\text{RS}}, \mathbf{x}_{i,t}^{\text{meteo}}] \quad (2)$$

where $\mathbf{x}_{i,t}^{\text{RS}}$ are remote sensing features (e.g. multispectral), $\mathbf{x}_{i,t}^{\text{meteo}}$ are gridded meteorological drivers;

- $\mathbf{y}_{i,t} \in \mathbb{R}^M$ is the target carbon flux observation at site i and time t , where M is the number of different fluxes to model;
- $\mathcal{T}_i \subseteq \mathcal{T}$ is the set of observation days available for site i .

The upscaling task accounts for spatial heterogeneity by conditioning predictions on both time-varying features and site-specific ecosystem context. The model learns a function $f_\theta : \mathbb{R}^F \times \mathcal{Z} \rightarrow \mathbb{R}^M$ that maps features and site metadata to carbon fluxes:

$$\hat{\mathbf{y}}_{i,t} = f_\theta(\mathbf{x}_{i,t}, \mathbf{z}_i) \quad (3)$$

where \mathbf{z}_i encodes the ecosystem (i.e. land cover) type and climate regime of the site i . This formulation explicitly recognizes that the relationship between drivers ($\mathbf{x}_{i,t}$) and fluxes ($\mathbf{y}_{i,t}$) varies systematically across ecosystems and climates.

Some models can explicitly leverage temporal dependencies by operating on a sliding window of past observations. For such models, the input at time t consists of a sequence of W consecutive days:

$$\mathbf{X}_{i,t}^{(W)} = [\mathbf{x}_{i,t-W+1}, \mathbf{x}_{i,t-W+2}, \dots, \mathbf{x}_{i,t}] \in \mathbb{R}^{W \times F} \quad (4)$$

and the prediction is made based on this temporal context:

$$\hat{\mathbf{y}}_{i,t} = f_\theta(\mathbf{X}_{i,t}^{(W)}, \mathbf{z}_i) \quad (5)$$

In *CarbonBench*, we recommend using of $W = 30$ days with a stride of 15 days for training of all the models with temporal context windows.

2.1.1 Zero-Shot Spatial Transfer. *CarbonBench* explicitly evaluates spatial generalization through a hold-out strategy that partitions sites rather than time steps. Let $\mathcal{S} = \{s_1, s_2, \dots, s_N\}$ denote the set of all flux tower sites. We define a partition:

$$\mathcal{S} = \mathcal{S}_{\text{train}} \cup \mathcal{S}_{\text{test}}, \quad \mathcal{S}_{\text{train}} \cap \mathcal{S}_{\text{test}} = \emptyset \quad (6)$$

Zero-shot transfer evaluates a model’s ability to generalize to completely unseen geographical locations:

$$\text{Train: } \mathcal{D}_{\text{train}} = \{(\mathbf{x}_i, \mathbf{z}_i, \mathbf{y}_{i,t}, t) \mid i \in \mathcal{S}_{\text{train}}, t \in \mathcal{T}_i\} \quad (7)$$

$$\text{Test: } \mathcal{D}_{\text{test}} = \{(\mathbf{x}_j, \mathbf{z}_j, \mathbf{y}_{j,t}, t) \mid j \in \mathcal{S}_{\text{test}}, t \in \mathcal{T}_j\} \quad (8)$$

During training, the model has access to feature vectors $\phi(\mathbf{x}, t)$ for all spatiotemporal locations, but carbon flux labels $\mathbf{y}_{j,t}$ are withheld for test sites $j \in \mathcal{S}_{\text{test}}$. At inference, the model must predict fluxes at test locations using only the learned representations from training sites and the available features at test sites.

2.1.2 Stratified Evaluation. To ensure comprehensive assessment across diverse ecosystems and climates, *CarbonBench* provides two stratified train-test splits:

IGBP-stratified split: Sites are partitioned based on the International Geosphere–Biosphere Programme (IGBP) vegetation type $v \in \mathcal{V}$ (16 classes: croplands, forests, grasslands, etc.), ensuring representation of all major ecosystem types:

$$\mathcal{S}_{\text{train}} = \bigcup_{v \in \mathcal{V}} \mathcal{S}_{\text{train}}^{(v)}, \quad \mathcal{S}_{\text{test}} = \bigcup_{v \in \mathcal{V}} \mathcal{S}_{\text{test}}^{(v)} \quad (9)$$

with approximately 80% of sites from each vegetation type allocated to training.

Köppen-stratified split: Sites are partitioned based on Köppen-Geiger climate class [8] $c \in \mathcal{C}$ (5 main classes: tropical, arid, temperate, continental, polar):

$$\mathcal{S}_{\text{train}} = \bigcup_{c \in \mathcal{C}} \mathcal{S}_{\text{train}}^{(c)}, \quad \mathcal{S}_{\text{test}} = \bigcup_{c \in \mathcal{C}} \mathcal{S}_{\text{test}}^{(c)} \quad (10)$$

This stratification enables fine-grained analysis of model performance across different environmental conditions and vegetation types, revealing which ecosystems or climates pose the greatest transfer learning challenges.

3 Related Work

Carbon flux upscaling efforts. The primary goal of carbon flux upscaling is to produce gridded estimates of terrestrial carbon exchange from sparse eddy covariance (EC) observations for climate modeling and decision-making. Most approaches model gross primary production (GPP), ecosystem respiration (RECO), and net ecosystem exchange (NEE) as functions of remotely sensed vegetation indicators and meteorological drivers. Notable operational products include FLUXCOM [17] and FLUXCOM-X-BASE [26], which combine multiple algorithmic families and multi-modal data to generate global flux estimates. Recent efforts have explored meta-learning [25], transfer learning with plant functional type specialization [48], and knowledge-guided approaches incorporating physics constraints [11]. Despite these advances, which can serve as stepping stones for new research existing studies differ substantially in their selection of sites, features, and evaluation protocols, making systematic comparison difficult. A detailed review of carbon flux upscaling methods is provided in Appendix B.

Transfer learning benchmarks in machine learning. While transfer learning has become central to modern ML, existing benchmarks exhibit critical gaps. Domain adaptation benchmarks (Office-31 [38], VisDA [32], DomainNet [31]) and NLP evaluation suites (GLUE [45]) predominantly focus on classification tasks. Transfer learning for regression, particularly time series regression remains underexplored. Existing time series benchmarks [14, 47, 49] evaluate temporal generalization (forecasting future values at known locations) rather than spatial transfer across geographically distinct domains. No benchmark systematically evaluates spatial generalization for time series regression, which happens to be of great importance in Earth system sciences [4, 35], ecology [19], and other scientific domains where observations are spatially sparse yet global predictions are needed. Scientific applications offer natural testbeds for spatial transfer learning, featuring genuine heterogeneity, interpretable physical features, and high societal impact, and yet this opportunity remains largely unexploited in the machine learning benchmarking ecosystem [19, 46]. LLM: **CarbonBench contribution.** CarbonBench directly addresses these gaps by providing the first benchmark for zero-shot spatial transfer learning in time series regression, grounded in the scientifically and societally critical problem of terrestrial carbon flux upscaling. By standardizing site selection, feature sets, and evaluation protocols, CarbonBench enables systematic comparison of transfer learning methods while bridging machine learning benchmarks with real-world scientific discovery. A comprehensive discussion of existing transfer learning benchmarks and their limitations is provided in Appendix B.

4 Methodology

In this section we describe the data sources used to create *CarbonBench*, domain-specific assumptions we made, the design of our pipeline and experiments.

4.1 Eddy Covariance

The ground truth in *CarbonBench* is derived from eddy covariance measurements obtained through major global and regional networks, including FLUXNET [2], AmeriFlux [28], ICOS [34], and JapanFlux [41]. The benchmark aggregates daily time series from 567 flux tower sites covering the period 2000–2024. These sites span all five main Köppen–Geiger climate classes (Fig. 7) and nearly all ecoregions defined by IGBP classification, excluding only the barren category. IGBP classes were extracted from the site auxiliary information.

Because EC data are inherently noisy, intermittent, and subject to site-specific post processing, we rely on fluxes standardized under the ONEFlux methodology [29]. This pipeline partitions the observed net flux into three key components, which serve as prediction targets in *CarbonBench*:

- GPP (GPP_NT_VUT_USTAR50): gross primary production, representing downward carbon flux due to photosynthesis; positive during daytime and zero at night.
- RECO (RECO_NT_VUT_USTAR50): ecosystem respiration, representing upward flux; positive at night and zero during the day.
- NEE (NEE_VUT_USTAR50): net ecosystem exchange, the balance between GPP and RECO; negative during daytime (uptake) and positive at night (release).

We also include NEE_VUT_USTAR50_QC (Fig. 8), a continuous binary quality-control flag (0 = lowest, 1 = highest quality). Higher QC values indicate a larger fraction of valid hourly observations contributing to the daily aggregate.

4.2 Remote Sensing Data

Vegetation properties are among the strongest determinants of terrestrial carbon fluxes, and satellite-based remote sensing enables systematic monitoring of these characteristics at the global scale. For *CarbonBench*, we use data from NASA’s Moderate Resolution Imaging Spectroradiometer (MODIS) onboard the Terra satellite.

The product used here is MOD09GA [44], which provides estimates of surface spectral reflectance corrected for atmospheric scattering and absorption at 500 m spatial and daily temporal resolution. We extracted seven spectral bands (Red, NIR, Blue, Green, SWIR1–3) and the corresponding cloud mask using Google Earth Engine (GEE) [15]. For each flux tower site, a 2 km × 2 km window was centered on the tower location, and mean reflectance values were computed. The cloud mask was converted into a binary variable (1 = cloud, 0 = clear), then averaged over the window to yield a continuous cloud fraction.

4.3 Meteorological Drivers

Meteorological conditions strongly influence terrestrial carbon dynamics by regulating photosynthesis, respiration, and evapotranspiration. CarbonBench incorporates climate variables from

To extend this observation, Figure 5 reports the mean and standard deviation of each target variable (GPP_NT_VUT_USTAR50, RECO_NT_VUT_USTAR50, NEE_VUT_USTAR50) aggregated by Köppen climate class along with the number of sites per climate type. The figures show that tropical regions exhibit the largest absolute mean flux values across all targets, despite being the second least represented climate classes in the EC network.

5 Experimental Design

5.1 Evaluation Metrics

We evaluate model performance using three metrics: coefficient of determination (R^2), root mean squared error (**RMSE**) in original flux units ($\text{gC m}^{-2} \text{day}^{-1}$), and normalized mean absolute error (**nMAE**) computed as mean absolute error normalized by site-level mean flux magnitude to enable fair comparison across sites with substantially different flux ranges. All metrics are computed per-site, then reported as quantiles (25th, 50th median, 75th percentile) across the test site distribution.

All test-set evaluations are performed exclusively on high-quality observations ($\text{NEE_VUT_USTAR50_QC} = 1$) to ensure reliable assessment, while training utilizes the full quality spectrum via the quality-weighted loss function described in Section 5.5.

5.2 Train-Test Split Strategy

The dataset exhibits substantial imbalance across both IGBP vegetation types and Köppen climate classes, with some categories represented by as few as two sites. To comprehensively evaluate spatial generalization across diverse environmental contexts, we design two complementary stratified train-test splits: one stratified by ecosystem type (IGBP) and one by climate regime (Köppen). This dual evaluation protocol ensures that model performance is assessed separately across both ecological and climatic gradients, revealing which dimension of environmental heterogeneity poses greater transfer learning challenges.

Table 1 summarizes the resulting site partitions. For each stratification scheme, models are trained and evaluated independently, enabling direct comparison of generalization difficulty across vegetation types versus climate zones.

IGBP-stratified split: Several vegetation classes (SNO, URB, WAT) are represented by only two sites each. To ensure meaningful evaluation for these rare categories while retaining sufficient training signal, we apply a **0.5/0.5** train-test split for IGBP types with ≤ 10 sites. For all other vegetation classes, we perform a standard **0.8/0.2** stratified split, yielding 448 training sites and 115 test sites.

Köppen-stratified split: Climate classes exhibit less severe imbalance than vegetation types, with the smallest class (Polar) containing 15 sites. We therefore apply a uniform **0.8/0.2** stratified split across all five climate zones, resulting in 453 training sites and 119 test sites.

By evaluating models under both splits, we can identify whether architectures generalize better across climate gradients, ecosystem types, or struggle equally with both dimensions of spatial heterogeneity.

Table 1: Train-test site partitions for IGBP vegetation (a) and Köppen climate (b) stratification schemes. All splits ensure representation of every category in both training and test sets despite severe class imbalance.

(a) IGBP split			
IGBP Class	Raw	Train	Test
Croplands (CRO)	70	56	14
Closed Shrublands (CSH)	9	5	4
Cropland/Natural Vegetation Mosaic (CVM)	4	2	2
Deciduous Broadleaf Forests (DBF)	83	66	17
Deciduous Needleleaf Forests (DNF)	12	10	2
Evergreen Broadleaf Forests (EBF)	21	17	4
Evergreen Needleleaf Forests (ENF)	125	100	25
Grasslands (GRA)	90	72	18
Mixed Forests (MF)	23	18	5
Open Shrublands (OSH)	36	29	7
Savannas (SAV)	12	9	3
Snow and Ice (SNO)	2	1	1
Urban and Built-up Lands (URB)	2	1	1
Water Bodies (WAT)	2	1	1
Permanent Wetlands (WET)	64	51	13
Woody Savannas (WSA)	12	10	2
Total	567	448	115

(b) Köppen climate split			
Köppen Class	Raw	Train	Test
Tropical (A)	19	15	4
Arid (B)	55	44	11
Temperate (C)	194	155	39
Continental (D)	284	227	57
Polar (E)	15	12	3
Total	567	453	119

5.3 Feature Sets

In total, *CarbonBench* includes 165 features, comprising MODIS-derived surface variables (12), site coordinates (latitude and longitude), and meteorological drivers from ERA5-Land (150). Many of these covariates are redundant, and using the full feature set can be computationally expensive, particularly when combined with long temporal windows. To balance flexibility and efficiency, we define three nested ERA5-Land feature sets.

- **Minimal (6 variables):** A compact set capturing the primary biophysical drivers of terrestrial carbon exchange, based on domain knowledge and feature selections from prior carbon flux upscaling studies [25, 36, 37]: 2-meter air temperature, total precipitation, surface net solar radiation, total evaporation, and leaf area indices for high and low vegetation. This configuration prioritizes the most direct controls on photosynthesis and respiration.
- **Standard (36):** an extended set that augments the minimal configuration with wind, air pressure, more detailed radiation, and soil variables.
- **Full (150):** the complete set of all ERA5-Land variables available via GEE.

The exact list of variables included in each feature set is provided in Appendix A. All experiments reported in this work use the **Minimal** feature set to establish baseline performance under the most constrained and computationally efficient setting.

5.4 Baseline Models

We evaluate two categories of baseline architectures: **static** models that operate on single time-step feature vectors, and **temporal** models that explicitly leverage sequential dependencies. All

models are trained in a multi-task setting to jointly predict GPP, RECO, and NEE. Static baselines operate on feature vectors of shape $(1, F)$, where F denotes the predictors for a single day. This category includes widely-used tree-based methods—XGBoost [5] and LightGBM [20]—which dominate carbon flux upscaling literature.

Temporal baselines capture sequential dependencies using sliding windows of $W = 30$ consecutive days with a stride of 15 days. We evaluate recurrent architectures including LSTM [16] and GRU [6], along with their concatenated-input variants CT-LSTM and CT-GRU, where categorical variables (IGBP type, Köppen class) are one-hot encoded and concatenated at each time step. We additionally consider transformer-based architectures: an encoder-only Transformer [42] and a Patch-Transformer based on PatchTST [27]. Finally, we include TAM-RL [36], a transfer-learning-specific architecture designed for cross-domain generalization in environmental applications.

5.5 Training Protocol

All neural network models are trained using a composite loss function incorporating quality weighting, class balancing, and physics-based flux balance constraints, as described in prior work [37]. Tree-based methods use analogous instance weighting for fair comparison. Hyperparameter optimization is performed via 5-fold cross-validation stratified by Köppen climate class, and final predictions are obtained by averaging across 10 models trained with different random seeds. Full details on the loss function formulation and hyperparameter configurations are provided in Appendix D.

6 Results

6.1 Zero-Shot Performance

Table 2 presents zero-shot transfer performance for ensemble models (10-seed average), with results reported as median site-level performance and interquartile range (subscript = 25th percentile, superscript = 75th percentile) across test sites. Temporal models (LSTM, CT-LSTM, Transformer, TAM-RL) outperform static tree-based baselines across all targets and stratification schemes. TAM-RL achieves best median GPP performance under IGBP stratification ($R^2 = 0.631$), while Transformer excels under Köppen ($R^2 = 0.709$).

Critically, TAM-RL demonstrates superior robustness with consistently higher 25th percentile performance. Under IGBP, TAM-RL’s GPP 25th percentile ($R^2 = 0.251$) exceeds CT-LSTM (0.235), LSTM (0.219), and Transformer (0.198), indicating fewer catastrophic failures. For RECO under Köppen, TAM-RL achieves 25th percentile $R^2 = 0.085$ versus negative values for most models (except LSTM: 0.079, CT-GRU: 0.093). This improved worst-case generalization is critical for reliable carbon flux predictions across all ecosystems. In contrast, standard models show negative 25th percentiles for NEE and RECO (e.g., XGBoost RECO under Köppen: 25th percentile = -0.601), meaning 25% of test sites perform worse than site-level mean prediction.

Net ecosystem exchange exhibits fundamentally poorer performance than GPP or RECO. The best model (CT-LSTM) achieves median $R^2 = 0.384$ [-0.145, 0.564] under Köppen, with 25% of sites showing negative R^2 . TAM-RL achieves comparable median

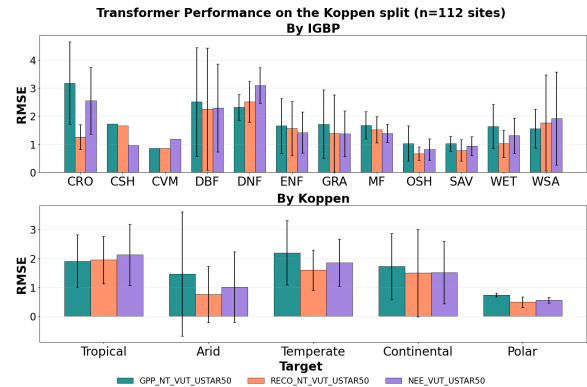


Figure 6: The average site-level RMSE of the transformer model on the Köppen split aggregated by IGBP and Köppen classes. The error bars represent one standard deviation. The bars without errors represent classes with only one EC site.

($R^2 = 0.340$) with narrower interquartile range. The nMAE values confirm NEE difficulty: median nMAE = 2.126–2.688 versus 0.385–0.419 for GPP (5–6× higher). This heterogeneity suggests NEE failures concentrate in regions where the small residual balance between GPP and RECO amplifies component errors.

6.2 Vegetation vs. Climate Stratification

The distribution of site-level performance differs notably between IGBP and Köppen stratification schemes. Under Köppen stratification, temporal models achieve higher median GPP performance (Transformer, Figure 6: median $R^2 = 0.709$ vs. 0.600 under IGBP), but the 25th percentile reveals more severe failures: Köppen 25th percentile $R^2 = 0.311$ vs. IGBP 25th percentile = 0.198. This indicates that while the typical site is predicted better under Köppen stratification, the worst-performing 25% of sites exhibit catastrophic failures under climate-based splits. For XGBoost under Köppen, the RECO 25th percentile reaches $R^2 = -0.601$, suggesting complete model failure at the most challenging sites (likely Tropical or Polar zones with extreme flux dynamics). The site-level interquartile ranges expose which stratification scheme poses greater challenges for robust spatial transfer. Köppen splits show wider IQR for RECO and NEE (e.g., CT-LSTM NEE IQR spans 0.709 units under Köppen vs. 0.477 units under IGBP), indicating that climate-driven distribution shifts create more variable site-level performance—some climate zones transfer well while others fail dramatically. In contrast, IGBP splits show more consistent but uniformly moderate performance across the site distribution. Future work should disaggregate these site-level metrics by individual IGBP classes and Köppen zones to identify which specific ecosystems and climates drive the poor 25th percentile performance, guiding targeted model improvements and field campaigns.

7 Discussions

Beyond serving as a benchmark for methodological comparison, *CarbonBench* is designed as a testbed for scientific discovery. Models developed and evaluated within this framework have the potential to improve operational carbon flux products used in climate policy and carbon accounting. At the same time, systematic analysis of where and why models succeed or fail in spatial transfer can yield insights that inform both machine learning

Table 2: Baseline zero-shot performance on *CarbonBench*. Results are averaged over an ensemble of 10 models trained with different random seeds. Arrows indicate the direction of improvement.

Split	Model	Targets								
		GPP			RECO			NEE		
		$R^2 \uparrow$	RMSE \downarrow	nMAE \downarrow	$R^2 \uparrow$	RMSE \downarrow	nMAE \downarrow	$R^2 \uparrow$	RMSE \downarrow	nMAE \downarrow
IGBP	XGBoost	0.495 ^{0.701} _{0.121}	1.833 ^{2.600} _{1.319}	0.522 ^{0.687} _{0.395}	0.330 ^{0.617} _{-0.093}	1.316 ^{1.933} _{0.967}	0.406 ^{0.654} _{0.310}	0.287 ^{0.496} _{-0.086}	1.340 ^{1.937} _{1.017}	2.105 ^{4.493} _{1.195}
	LightGBM	0.537 ^{0.779} _{0.201}	1.611 ^{2.585} _{1.226}	0.440 ^{0.675} _{0.308}	0.464 ^{0.710} _{-0.215}	1.209 ^{1.802} _{0.817}	0.376 ^{0.542} _{0.268}	0.335 ^{0.542} _{0.123}	1.340 ^{1.882} _{0.847}	2.058 ^{4.106} _{1.098}
	LSTM	0.582 ^{0.780} _{0.219}	1.571 ^{2.454} _{1.091}	0.417 ^{0.630} _{0.312}	0.414 ^{0.728} _{-0.293}	1.229 ^{1.784} _{0.776}	0.345 ^{0.604} _{0.272}	0.315 ^{0.512} _{-0.060}	1.303 ^{1.995} _{0.910}	1.846 ^{4.093} _{1.108}
	CT-LSTM	0.614 ^{0.795} _{0.235}	1.578 ^{2.538} _{1.120}	0.400 ^{0.633} _{0.301}	0.406 ^{0.750} _{-0.317}	1.202 ^{1.754} _{0.821}	0.367 ^{0.584} _{0.256}	0.28 ^{0.481} _{-0.004}	1.337 ^{2.048} _{1.018}	2.056 ^{4.593} _{1.162}
	GRU	0.520 ^{0.733} _{0.138}	1.658 ^{2.659} _{1.190}	0.46 ^{0.609} _{0.353}	0.389 ^{0.708} _{-0.273}	1.273 ^{1.747} _{0.823}	0.369 ^{0.558} _{0.288}	0.28 ^{0.441} _{-0.025}	1.344 ^{2.087} _{1.028}	1.985 ^{4.004} _{1.182}
	CT-GRU	0.559 ^{0.790} _{0.243}	1.668 ^{2.534} _{1.157}	0.41 ^{0.649} _{0.323}	0.321 ^{0.732} _{-0.448}	1.245 ^{1.857} _{0.843}	0.375 ^{0.598} _{0.273}	0.284 ^{0.467} _{0.013}	1.440 ^{2.021} _{1.028}	2.095 ^{4.876} _{1.271}
	Transformer	0.600 ^{0.801} _{0.198}	1.679 ^{2.684} _{1.138}	0.413 ^{0.623} _{0.310}	0.376 ^{0.737} _{-0.498}	1.269 ^{1.887} _{0.823}	0.386 ^{0.603} _{0.265}	0.288 ^{0.489} _{-0.103}	1.433 ^{2.015} _{1.018}	2.134 ^{4.442} _{1.231}
	Patch-Transformer	0.487 ^{0.743} _{0.042}	1.806 ^{2.714} _{1.397}	0.44 ^{0.630} _{0.344}	0.309 ^{0.696} _{-0.758}	1.322 ^{1.880} _{0.901}	0.400 ^{0.606} _{0.292}	0.116 ^{0.367} _{-0.214}	1.486 ^{1.982} _{1.100}	2.064 ^{4.647} _{1.242}
	TAM-RL	0.631 ^{0.810} _{0.251}	1.594 ^{2.671} _{1.090}	0.385 ^{0.595} _{0.297}	0.459 ^{0.761} _{-0.411}	1.173 ^{1.703} _{0.798}	0.362 ^{0.558} _{0.258}	0.32 ^{0.504} _{0.053}	1.334 ^{1.926} _{0.906}	1.916 ^{4.545} _{1.143}
Köppen	XGBoost	0.419 ^{0.645} _{-0.119}	2.098 ^{2.837} _{1.475}	0.541 ^{0.813} _{0.409}	0.216 ^{0.577} _{-0.601}	1.475 ^{2.077} _{1.146}	0.411 ^{0.635} _{0.320}	0.096 ^{0.374} _{-0.336}	1.526 ^{2.239} _{1.094}	2.688 ^{4.467} _{1.369}
	LightGBM	0.605 ^{0.786} _{0.265}	1.618 ^{2.224} _{1.034}	0.410 ^{0.613} _{0.291}	0.500 ^{0.737} _{0.107}	1.116 ^{1.688} _{0.760}	0.348 ^{0.463} _{0.262}	0.351 ^{0.528} _{-0.147}	1.275 ^{2.006} _{0.810}	2.330 ^{4.823} _{1.215}
	LSTM	0.635 ^{0.807} _{0.329}	1.591 ^{2.251} _{1.032}	0.410 ^{0.547} _{0.298}	0.450 ^{0.744} _{0.079}	1.124 ^{1.827} _{0.780}	0.349 ^{0.498} _{0.273}	0.284 ^{0.559} _{-0.228}	1.281 ^{2.068} _{0.910}	2.449 ^{4.861} _{1.306}
	CT-LSTM	0.687 ^{0.818} _{0.327}	1.478 ^{2.150} _{0.925}	0.40 ^{0.528} _{0.288}	0.467 ^{0.768} _{0.062}	1.083 ^{1.742} _{0.729}	0.334 ^{0.461} _{0.255}	0.384 ^{0.564} _{0.145}	1.182 ^{1.864} _{0.796}	2.126 ^{4.830} _{1.217}
	GRU	0.666 ^{0.786} _{0.342}	1.676 ^{2.275} _{1.032}	0.400 ^{0.582} _{0.311}	0.458 ^{0.703} _{-0.194}	1.169 ^{1.840} _{0.811}	0.368 ^{0.513} _{0.284}	0.266 ^{0.555} _{-0.330}	1.374 ^{2.082} _{0.925}	2.630 ^{4.992} _{1.282}
	CT-GRU	0.665 ^{0.813} _{0.226}	1.599 ^{2.134} _{0.981}	0.410 ^{0.571} _{0.308}	0.460 ^{0.735} _{0.093}	1.080 ^{1.547} _{0.707}	0.353 ^{0.481} _{0.262}	0.320 ^{0.510} _{-0.189}	1.337 ^{2.067} _{0.845}	2.476 ^{5.141} _{1.185}
	Transformer	0.709 ^{0.804} _{0.311}	1.554 ^{2.181} _{0.921}	0.396 ^{0.535} _{0.296}	0.464 ^{0.730} _{-0.089}	1.163 ^{1.679} _{0.780}	0.356 ^{0.458} _{0.260}	0.331 ^{0.565} _{-0.212}	1.265 ^{1.898} _{0.849}	2.190 ^{4.940} _{1.183}
	Patch-Transformer	0.589 ^{0.760} _{0.218}	1.724 ^{2.464} _{1.034}	0.458 ^{0.594} _{0.333}	0.439 ^{0.704} _{-0.088}	1.137 ^{1.726} _{0.799}	0.364 ^{0.490} _{0.286}	0.200 ^{0.375} _{-0.230}	1.455 ^{2.359} _{0.945}	2.702 ^{5.100} _{1.324}
	TAM-RL	0.692 ^{0.816} _{0.376}	1.505 ^{2.202} _{0.947}	0.40 ^{0.547} _{0.284}	0.480 ^{0.756} _{0.085}	1.081 ^{1.602} _{0.725}	0.340 ^{0.474} _{0.261}	0.340 ^{0.556} _{-0.166}	1.266 ^{1.912} _{0.866}	2.315 ^{4.676} _{1.247}

research and the design of future ecological field campaigns. Below, we outline a set of key research opportunities enabled by CarbonBench, spanning model design, evaluation, uncertainty, and knowledge integration.

(1) *Feature engineering and selection*: While *CarbonBench* provides a rigorous evaluation framework, all baseline experiments use only the Minimal (6-variable) feature set. Our preliminary evaluations suggest that richer feature representations, particularly when combined with data-hungry architectures like Transformers, show promise for improving spatial generalization on average. However, we deliberately restrict baselines to the Minimal set to ensure computational tractability and establish a consistent foundation; systematic exploration of Standard and Full feature sets is left to future users of the benchmark. In addition, temporal models use a fixed 30-day input window, but the role of the window length should be investigated separately as it may vary by ecosystem or season. (2) *Stratified and biome-specific evaluation*: Rather than improving purely site-averaged metrics, future work should focus on performance broken down by individual IGBP types and Köppen classes. This research may reveal which ecosystems pose the greatest transfer challenges and whether models exhibit systematic biases (e.g., overpredicting in tropics, underpredicting in polar regions). Such an analysis is essential for identifying where improved models or targeted data collection are most needed. (3) *Quality-aware modeling*: The default loss function provided in *CarbonBench* downsamples observations with lower quality and the models are tested on the observations of the highest quality. Investigating if architectures can be designed to weight predictions by expected reliability is a perspective direction. Moreover, the remote sensing drivers

were gap-filled leading to low-quality samples which require additional analysis of error propagation. (4) *Beyond TAM-RL, our baselines use standard supervised learning. Can adversarial domain adaptation, domain-invariant representations, or multi-source transfer learning improve zero-shot generalization to underrepresented biomes? Do they perform better spatial transfer compared to classical supervised methods?* (5) *Uncertainty quantification*: In *CarbonBench*, we intentionally use ensembles of baselines trained with different seeds to account for model uncertainty due to initializations. However, broader questions need to be asked: How confident are predictions in data-sparse regions? Could Bayesian neural networks, conformal prediction, or ensemble diversity metrics provide distribution-free uncertainty estimates critical for carbon accounting applications? (6) *Mixture of experts*: Baselines predict three carbon fluxes across all ecosystem types and are exposed to all ecosystem and climate types. Yet, it is not clear if there is a negative transfer of information between targets or contexts. So another perspective research question is can training a climate/ecosystem-specific model yield a better result? (7) *Self-supervised learning and auxiliary tasks*: Given the rise of foundation models and self-supervised learning, pretraining on unlabeled satellite time series (e.g., masked autoencoding, contrastive learning) and auxiliary prediction tasks (vegetation indices, soil moisture, phenology) could leverage the vast spatial-temporal coverage of remote sensing data beyond the limited labeled flux tower sites. (8) *Explainability and failure analysis*: Feature attribution methods (SHAP, integrated gradients) can reveal which environmental drivers dominate in different ecosystems and identify systematic failure modes. Analysis of prediction failures i.e. which sites, seasons, or flux components exhibit largest errors can prioritize field campaign locations and guide strategic expansion of flux tower networks to undersampled

regions. (9) Knowledge-guided ML: The existing land surface and biogeochemical process-based models (e.g. MiCASA, CMIP6 and others) having global spatial and significant temporal coverage are ideal candidates for pre-training of the ML models with later fine-tuning on the ground-true EC observations. This direction can be combined with ideas of likelihood inference, surrogate modeling, physics-informed priors and inductive biases and therefore are a very promising direction of research.

8 Conclusion

We introduce *CarbonBench*, the first benchmark for spatial transfer learning in carbon flux upscaling, providing 567 eddy covariance sites with satellite and meteorological features, dual stratified evaluation protocols (IGBP vegetation and Köppen climate), and reproducible baseline implementations. Our zero-shot evaluation reveals that temporal models outperform static baselines, with TAM-RL achieving not only competitive median performance but critically improved robustness through consistently higher 25th percentile metrics, indicating fewer catastrophic failures at challenging sites. This demonstrates that architectures explicitly designed for cross-domain generalization can improve worst-case spatial transfer—essential for reliable carbon monitoring across all ecosystems. However, all models struggle with NEE prediction and exhibit severe degradation on underrepresented biomes, with climate-stratified evaluation proving more challenging for robust generalization.

Beyond carbon science, *CarbonBench* addresses a critical gap in ML benchmarking: spatial transfer learning for time series regression. By providing quantile-based evaluation that exposes tail performance rather than masking failures through averaging, *CarbonBench* enables rigorous assessment of spatial transfer robustness. The benchmark is publicly available, and we encourage the community to extend it with new methods and conduct stratified per-biome analysis to identify systematic failures in underrepresented ecosystems.

References

- [1] Peyman Babakhani, Tanapon Phenrat, Mohammed Baalousha, Kullapa Soratana, Caroline L Peacock, Benjamin S Twining, and Michael F Hochella Jr. 2022. Potential use of engineered nanoparticles in ocean fertilization for large-scale atmospheric carbon dioxide removal. *Nature Nanotechnology* 17, 12 (2022), 1342–1351.
- [2] Dennis Baldocchi, Eva Falge, Lianhong Gu, Richard Olson, David Hollinger, Steve Running, Peter Anthoni, Ch Bernhofer, Kenneth Davis, Robert Evans, et al. 2001. FLUXNET: A new tool to study the temporal and spatial variability of ecosystem-scale carbon dioxide, water vapor, and energy flux densities. *Bulletin of the American Meteorological Society* 82, 11 (2001), 2415–2434.
- [3] Dennis D Baldocchi. 2003. Assessing the eddy covariance technique for evaluating carbon dioxide exchange rates of ecosystems: past, present and future. *Global change biology* 9, 4 (2003), 479–492.
- [4] Gustau Camps-Valls, Devis Tuia, Xiao Xiang Zhu, and Markus Reichstein. 2021. *Deep learning for the Earth Sciences: A comprehensive approach to remote sensing, climate science and geosciences*. John Wiley & Sons.
- [5] Tianqi Chen and Carlos Guestrin. 2016. Xgboost: A scalable tree boosting system. In *Proceedings of the 22nd acm sigkdd international conference on knowledge discovery and data mining*. 785–794.
- [6] Kyunghyun Cho, Bart Van Merriënboer, Caglar Gulcehre, Dzmitry Bahdanau, Fethi Bougares, Holger Schwenk, and Yoshua Bengio. 2014. Learning phrase representations using RNN encoder-decoder for statistical machine translation. *arXiv preprint arXiv:1406.1078* (2014).
- [7] Housen Chu, Xiangzhong Luo, Zutao Ouyang, W Stephen Chan, Sigrid Dengel, Sébastien C Biraud, Margaret S Torn, Stefan Metzger, Jitendra Kumar, M Altaf Arain, et al. 2021. Representativeness of Eddy-Covariance flux footprints for areas surrounding AmeriFlux sites. *Agricultural and Forest Meteorology* 301 (2021), 108350.
- [8] D. Cui, S. Liang, D. Wang, and Z. Liu. 2021. A 1 km global dataset of historical (1979–2013) and future (2020–2100) Köppen–Geiger climate classification and bioclimatic variables. *Earth System Science Data* 13, 11 (2021), 5087–5114. doi:10.5194/essd-13-5087-2021
- [9] Jia Deng, Wei Dong, Richard Socher, Li-Jia Li, Kai Li, and Li Fei-Fei. 2009. Imagenet: A large-scale hierarchical image database. In *2009 IEEE conference on computer vision and pattern recognition*. Ieee, 248–255.
- [10] Dheeru Dua and Casey Graff. 2017. UCI Machine Learning Repository. <http://archive.ics.uci.edu/ml>
- [11] Bin Fan, Hankui K Zhang, Zhongbin B Li, Jingfeng Xiao, Xianghong Che, Zhihua Liu, Gustau Camps-Valls, and Jing M Chen. 2025. Estimating carbon fluxes over North America using a physics-constrained deep learning model. *ISPRS Journal of Photogrammetry and Remote Sensing* 227 (2025), 551–569.
- [12] Samer Fawzy, Ahmed I Osman, Haiping Yang, John Doran, and David W Rooney. 2021. Industrial biochar systems for atmospheric carbon removal: a review. *Environmental Chemistry Letters* 19, 4 (2021), 3023–3055.
- [13] Yong Ge, Yan Jin, Alfred Stein, Yuehong Chen, Jianghao Wang, Jinfeng Wang, Qiuming Cheng, Hexiang Bai, Mengxiao Liu, and Peter M Atkinson. 2019. Principles and methods of scaling geospatial Earth science data. *Earth-Science Reviews* 197 (2019), 102897.
- [14] Rakshitha Godahewa, Christoph Bergmeir, Geoffrey I Webb, Rob J Hyndman, and Pablo Montero-Manso. 2021. Monash time series forecasting archive. *arXiv preprint arXiv:2105.06643* (2021).
- [15] Noel Gorelick, Matt Hancher, Mike Dixon, Simon Ilyushchenko, David Thau, and Rebecca Moore. 2017. Google Earth Engine: Planetary-scale geospatial analysis for everyone. *Remote sensing of Environment* 202 (2017), 18–27.
- [16] Sepp Hochreiter and Jürgen Schmidhuber. 1997. Long short-term memory. *Neural computation* 9, 8 (1997), 1735–1780.
- [17] Martin Jung, Christopher Schwalm, Mirco Migliavacca, Sophia Walther, Gustau Camps-Valls, Sujun Koirala, Peter Anthoni, Simon Besnard, Paul Bodesheim, Nuno Carvalhais, et al. 2020. Scaling carbon fluxes from eddy covariance sites to globe: synthesis and evaluation of the FLUXCOM approach. *Biogeosciences* 17, 5 (2020), 1343–1365.
- [18] Andreas Kamilaris and Francesc X Prenafeta-Boldú. 2018. Deep learning in agriculture: A survey. *Computers and electronics in agriculture* 147 (2018), 70–90.
- [19] Anuj Karpatne, Gowtham Atluri, James H Faghmous, Michael Steinbach, Arindam Banerjee, Auroop Ganguly, Shashi Shekhar, Nagiza Samatova, and Vipin Kumar. 2017. Theory-guided data science: A new paradigm for scientific discovery from data. *IEEE Transactions on knowledge and data engineering* 29, 10 (2017), 2318–2331.
- [20] Guolin Ke, Qi Meng, Thomas Finley, Taifeng Wang, Wei Chen, Weidong Ma, Qiwei Ye, and Tie-Yan Liu. 2017. Lightgbm: A highly efficient gradient boosting decision tree. *Advances in neural information processing systems* 30 (2017).
- [21] Alex Krizhevsky, Geoffrey Hinton, et al. 2009. Learning multiple layers of features from tiny images. (2009).
- [22] Yann LeCun, Corinna Cortes, and CJ Burges. 2010. MNIST handwritten digit database. *ATT Labs [Online]*. Available: <http://yann.lecun.com/exdb/mnist> 2 (2010).
- [23] Valérie Masson-Delmotte, Panmao Zhai, Anna Pirani, Sarah L Connors, Clotilde Péan, Sophie Berger, Nada Caud, Yang Chen, Leah Goldfarb, Melissa I Gomis, et al. 2023. Summary for policymakers. *Climate change 2021: The physical science basis. Contribution of working group I to the sixth assessment report of the intergovernmental panel on climate change* (2023), 3–32.
- [24] Joaquín Muñoz-Sabater, Emanuel Dutra, Anna Agustí-Panareda, Clément Albergel, Gabriele Arduini, Gianpaolo Balsamo, Souhail Boussetta, Margarita Choulga, Shaun Harrigan, Hans Hersbach, et al. 2021. ERA5-Land: A state-of-the-art global reanalysis dataset for land applications. *Earth system science data* 13, 9 (2021), 4349–4383.
- [25] Juan Nathaniel, Jianguo Liu, and Pierre Gentine. 2023. MetaFlux: Meta-learning global carbon fluxes from sparse spatiotemporal observations. *Scientific Data* 10, 1 (2023), 440.
- [26] Jacob A Nelson, Sophia Walther, Fabian Gans, Basil Kraft, Ulrich Weber, Kimberly Novick, Nina Buchmann, Mirco Migliavacca, Georg Wohlfahrt, Ladislav Šigut, et al. 2024. X-BASE: the first terrestrial carbon and water flux products from an extended data-driven scaling framework, FLUXCOM-X. *Biogeosciences* 21, 22 (2024), 5079–5115.
- [27] Y Nie. 2022. A Time Series is Worth 64Words: Long-term Forecasting with Transformers. *arXiv preprint arXiv:2211.14730* (2022).
- [28] Kimberly Ann Novick, JA Biederman, AR Desai, ME Litvak, David JP Moore, RL Scott, and MS Torn. 2018. The AmeriFlux network: A coalition of the willing. *Agricultural and Forest Meteorology* 249 (2018), 444–456.
- [29] Gilberto Pastorello, Carlo Trotta, Eleonora Canfora, Housen Chu, Danielle Christianson, You-Wei Cheah, Cristina Poindexter, Jiquan Chen, Abdelrahman Elbashaandy, Marty Humphrey, et al. 2020. The FLUXNET2015 dataset and the ONEFlux processing pipeline for eddy covariance data. *Scientific data* 7, 1 (2020), 225.

- [30] Adam Paszke, Sam Gross, Francisco Massa, Adam Lerer, James Bradbury, Gregory Chanan, Trevor Killeen, Zeming Lin, Natalia Gimelshein, Luca Antiga, et al. 2019. Pytorch: An imperative style, high-performance deep learning library. *Advances in neural information processing systems* 32 (2019).
- [31] Xingchao Peng, Qinxun Bai, Xide Xia, Zijun Huang, Kate Saenko, and Bo Wang. 2019. Moment matching for multi-source domain adaptation. In *Proceedings of the IEEE/CVF international conference on computer vision*. 1406–1415.
- [32] Xingchao Peng, Ben Usman, Neela Kaushik, Judy Hoffman, Dequan Wang, and Kate Saenko. 2017. Visda: The visual domain adaptation challenge. *arXiv preprint arXiv:1710.06924* (2017).
- [33] Pranav Rajpurkar, Jian Zhang, Konstantin Lopyrev, and Percy Liang. 2016. Squad: 100,000+ questions for machine comprehension of text. *arXiv preprint arXiv:1606.05250* (2016).
- [34] Corinna Rebmann, Marc Aubinet, Hape Schmid, Nicola Arriga, Mika Aurela, George Burba, Robert Clement, Anne De Ligne, Gerardo Fratini, Bert Gielen, et al. 2018. ICOS eddy covariance flux-station site setup: a review. *International Agrophysics* 32, 4 (2018), 471–494.
- [35] Markus Reichstein, Gustau Camps-Valls, Bjorn Stevens, Martin Jung, Joachim Denzler, Nuno Carvalhais, and F Prabhat. 2019. Deep learning and process understanding for data-driven Earth system science. *Nature* 566, 7743 (2019), 195–204.
- [36] Arvind Renganathan, Rahul Ghosh, Ankush Khandelwal, and Vipin Kumar. 2025. Task Aware Modulation using Representation Learning: An Approach for Few Shot Learning in Environmental Systems. In *Proceedings of the 2025 SIAM International Conference on Data Mining (SDM)*. SIAM, 11–20.
- [37] Aleksei Rozanov, Arvind Renganathan, and Vipin Kumar. 2025. Task Aware Modulation using Representation Learning for Upscaling of Terrestrial Carbon Fluxes. *arXiv preprint* (2025).
- [38] Kate Saenko, Brian Kulis, Mario Fritz, and Trevor Darrell. 2010. Adapting visual category models to new domains. In *European conference on computer vision*. Springer, 213–226.
- [39] Han Lin Shang and Ruofan Xu. 2021. Regional forecasting of COVID-19 caseload by non-parametric regression: a VAR epidemiological model. *PLOS ONE* 16, 3 (2021), e0247428.
- [40] Steve Smith, Oliver Geden, Matthew Gidden, W Lamb, G Nemet, Jan Minx, Holly Buck, Josh Burke, Emily Cox, Morgan Edwards, et al. 2024. The state of carbon dioxide removal. (2024).
- [41] Masahito Ueyama, Yuta Takao, Hiromi Yazawa, Makiko Tanaka, Hironori Yabuki, Tomo'omi Kumagai, Hiroki Iwata, Md Abdul Awal, Mingyuan Du, Yoshinobu Harazono, et al. 2025. The JapanFlux2024 dataset for eddy covariance observations covering Japan and East Asia from 1990 to 2023. *Earth System Science Data* 17, 8 (2025), 3807–3833.
- [42] Ashish Vaswani, Noam Shazeer, Niki Parmar, Jakob Uszkoreit, Llion Jones, Aidan N Gomez, Lukasz Kaiser, and Illia Polosukhin. 2017. Attention is all you need. *Advances in neural information processing systems* 30 (2017).
- [43] Hemanth Venkateswara, Jose Eusebio, Shayok Chakraborty, and Sethuraman Panchanathan. 2017. Deep hashing network for unsupervised domain adaptation. In *Proceedings of the IEEE conference on computer vision and pattern recognition*. 5018–5027.
- [44] E. Vermote and R. Wolfe. 2015. *MOD09GA MODIS/Terra Surface Reflectance Daily L2G Global 1 km and 500 m SIN Grid V006*. doi:10.5067/MODIS/MOD09GA.006
- [45] Alex Wang, Amanpreet Singh, Julian Michael, Felix Hill, Omer Levy, and Samuel Bowman. 2018. GLUE: A multi-task benchmark and analysis platform for natural language understanding. In *Proceedings of the 2018 EMNLP workshop BlackboxNLP: Analyzing and interpreting neural networks for NLP*. 353–355.
- [46] Jared Willard, Xiaowei Jia, Shaoming Xu, Michael Steinbach, and Vipin Kumar. 2022. Integrating scientific knowledge with machine learning for engineering and environmental systems. *Comput. Surveys* 55, 4 (2022), 1–37.
- [47] Haixu Wu, Jiehui Xu, Jianmin Wang, and Mingsheng Long. 2021. Auto-former: Decomposition transformers with auto-correlation for long-term series forecasting. *Advances in neural information processing systems* 34 (2021), 22419–22430.
- [48] Qiwang Yuan, Xufeng Wang, Tao Che, and Jun Li. 2025. Global carbon flux dataset generated by fusing remote sensing and multiple flux networks observation. *Scientific Data* 12, 1 (2025), 1359.
- [49] Haoyi Zhou, Shanghang Zhang, Jieqi Peng, Shuai Zhang, Jianxin Li, Hui Xiong, and Wancai Zhang. 2021. Informer: Beyond efficient transformer for long sequence time-series forecasting. In *Proceedings of the AAAI conference on artificial intelligence*, Vol. 35. 11106–11115.

A Features Provided in CarbonBench

We use three feature sets of varying complexity for our experiments. All feature sets include MODIS reflectance bands and

observation geometry features in addition to the ERA5-Land variables listed below.

A.1 MODIS Features (Common to All Sets)

All feature sets include the following MODIS MOD09GA (Collection 6.1) features²:

- **Surface reflectance bands:** sur_refl_b01, sur_refl_b02, sur_refl_b03, sur_refl_b04, sur_refl_b05, sur_refl_b06, sur_refl_b07
- **Observation geometry:** SensorZenith, SensorAzimuth, SolarZenith, SolarAzimuth
- **Cloud mask:** clouds (custom binary ratio: 0 = clear, 1 = fully cloudy)

A.2 ERA5-Land Feature Sets

The following ERA5-Land Daily Aggregated variables³ are used across three feature set configurations.

A.2.1 Minimal (6 variables).

- temperature_2m
- total_precipitation_sum
- surface_net_solar_radiation_sum
- total_evaporation_sum
- leaf_area_index_high_vegetation
- leaf_area_index_low_vegetation

A.2.2 Standard (36 variables).

- temperature_2m
- total_precipitation_sum
- surface_net_solar_radiation_sum
- total_evaporation_sum
- leaf_area_index_high_vegetation
- leaf_area_index_low_vegetation
- dewpoint_temperature_2m
- skin_temperature
- soil_temperature_level_1
- soil_temperature_level_2
- soil_temperature_level_3
- soil_temperature_level_4
- volumetric_soil_water_layer_1
- volumetric_soil_water_layer_2
- volumetric_soil_water_layer_3
- volumetric_soil_water_layer_4
- u_component_of_wind_10m
- v_component_of_wind_10m
- surface_pressure
- snow_albedo
- snow_cover
- snow_density
- snow_depth
- snow_depth_water_equivalent
- skin_reservoir_content
- forecast_albedo

²https://developers.google.com/earth-engine/datasets/catalog/MODIS_061_MOD09GA

³https://developers.google.com/earth-engine/datasets/catalog/ECMWF_ERA5_LAND_DAILY_AGGR

- surface_latent_heat_flux_sum
- surface_net_thermal_radiation_sum
- surface_sensible_heat_flux_sum
- surface_solar_radiation_downwards_sum
- surface_thermal_radiation_downwards_sum
- evaporation_from_bare_soil_sum
- evaporation_from_the_top_of_canopy_sum
- evaporation_from_vegetation_transpiration_sum
- potential_evaporation_sum
- runoff_sum

A.2.3 Full (150 variables).

- dewpoint_temperature_2m
- temperature_2m
- skin_temperature
- soil_temperature_level_1
- soil_temperature_level_2
- soil_temperature_level_3
- soil_temperature_level_4
- lake_bottom_temperature
- lake_ice_depth
- lake_ice_temperature
- lake_mix_layer_depth
- lake_mix_layer_temperature
- lake_shape_factor
- lake_total_layer_temperature
- snow_albedo
- snow_cover
- snow_density
- snow_depth
- snow_depth_water_equivalent
- snowfall_sum
- snowmelt_sum
- temperature_of_snow_layer
- skin_reservoir_content
- volumetric_soil_water_layer_1
- volumetric_soil_water_layer_2
- volumetric_soil_water_layer_3
- volumetric_soil_water_layer_4
- forecast_albedo
- surface_latent_heat_flux_sum
- surface_net_solar_radiation_sum
- surface_net_thermal_radiation_sum
- surface_sensible_heat_flux_sum
- surface_solar_radiation_downwards_sum
- surface_thermal_radiation_downwards_sum
- evaporation_from_bare_soil_sum
- evaporation_from_open_water_surfaces_excluding_oceans_sum
- evaporation_from_the_top_of_canopy_sum
- evaporation_from_vegetation_transpiration_sum
- potential_evaporation_sum
- runoff_sum
- snow_evaporation_sum
- sub_surface_runoff_sum
- surface_runoff_sum
- total_evaporation_sum

- u_component_of_wind_10m
- v_component_of_wind_10m
- surface_pressure
- total_precipitation_sum
- leaf_area_index_high_vegetation
- leaf_area_index_low_vegetation

All variables in the full set include both base values and their `_min/_max` variants, resulting in 150 total features.

B Extended Related Work

This appendix provides a comprehensive review of (1) carbon flux upscaling methods and operational products, and (2) transfer learning benchmarks in machine learning, expanding on the brief overview in Section 3.

B.1 Carbon Flux Upscaling: Methods and Products

The primary goal of carbon flux upscaling is to produce improved gridded estimates of terrestrial carbon exchange for climate modeling and decision-making. Given the extensive existing literature, we do not attempt to exhaustively review all prior efforts, instead, we note that most approaches follow a common strategy. Specifically, they rely on target variables derived from global eddy covariance (EC) networks such as FLUXNET [2] and AmeriFlux [28], and estimate gross primary production (GPP; downward carbon flux), ecosystem respiration (RECO; upward carbon flux), and net ecosystem exchange (NEE; net balance), either individually or jointly in a multitask learning setting. These quantities are typically modeled as functions of remotely sensed vegetation indicators and gridded meteorological drivers at the target locations.

One of the most significant and earliest efforts in this domain is FLUXCOM [17] and its recent successor FLUXCOM-X-BASE [26]. The FLUXCOM framework integrates multiple algorithmic families, including kernel methods, neural networks, tree-based models, and regression splines, and is trained under two configurations: (a) a Remote Sensing (RS) setup using only multispectral remote sensing observations at 8-day temporal and 0.0833° spatial resolution, and (b) an RS+Meteo setup using additional daily meteorological variables at 0.5° spatial resolution. The newer FLUXCOM-X-BASE leverages the Extreme Gradient Boosting (XGBoost) [5] architecture combined with MODIS and climate forcings to generate global flux estimates at hourly temporal and 0.05° spatial resolution, achieving notable improvements over the original FLUXCOM product.

Another recent dataset, MetaFlux [25], introduces a meta-learning framework for carbon flux upscaling using deep learning architectures. The model operates in two stages: meta-training on base tasks with abundant samples (e.g., the sites in continental climates), followed by meta-updating on data-sparse tasks (e.g., tropical sites). Like FLUXCOM, MetaFlux relies on meteorological and MODIS-derived features, providing daily and monthly flux estimates at 0.25° spatial and 1d temporal resolution for 2001–2021.

Later, [48] proposed an alternative transfer learning strategy based on the XGBoost architecture. Their approach first trains a

universal base model using all available samples and predictors, followed by fine-tuning specialized models on subsets of data corresponding to distinct plant functional types (PFTs). This framework was used to produce GloFlux, a global carbon flux dataset at 0.1° spatial and monthly temporal resolution. In parallel, knowledge-guided machine learning (KGML) approaches have gained increasing attention in recent years. A study by [11] applied a transformer-based model [42] to upscale carbon fluxes over the United States at 500 m spatial and annual temporal resolution. The proposed method incorporated a physics-inspired loss function enforcing the carbon balance constraint, $NEE = RECO - GPP$. The authors reported that introducing this constraint led to RMSE reductions of 1.5–3.5%, demonstrating the potential benefits of embedding domain knowledge into learning objectives.

Despite these methodological advances, existing studies differ substantially in their selection of EC sites, target variables, feature sets, evaluation protocols, and performance metrics. This heterogeneity makes it difficult to assess whether reported improvements reflect genuine methodological progress or are artifacts of dataset and experimental design choices. Therefore, a standardized benchmark that bridges the machine learning and carbon flux research communities is essential for enabling transparent comparison and accelerating future progress.

B.2 Transfer Learning Benchmarks in Machine Learning

While transfer learning has become a cornerstone of modern machine learning, existing benchmarks exhibit notable gaps that limit progress in certain application domains.

Classification-dominated landscape: The majority of transfer learning benchmarks focus on classification tasks. In computer vision, unprecedented growth has been driven by standardized benchmarks [9, 21, 22] that enable systematic methodological comparison. Domain adaptation benchmarks such as Office-31 [38], Office-Home [43], VisDA [32], and DomainNet [31] evaluate cross-domain image classification. In NLP, benchmarks like GLUE [45], and SQuAD [33] primarily assess classification and span prediction tasks.

Limited regression benchmarks: Transfer learning for regression remains underexplored in the benchmarking literature. Regression under domain shift presents distinct challenges absent in classification: continuous predictions across varying scales, preservation of calibration, and sensitivity to distributional changes in target variables. The few existing regression benchmarks (e.g., UCI datasets [10] with artificial domain shifts) lack the scale, diversity, and real-world complexity needed to drive methodological innovation. This is especially true and more difficult and complex when considering time series regression.

Time series adds another layer of complexity: While some benchmarks address time series forecasting, including the Monash Time Series Forecasting Archive [14], Informer [49], and Autoformer [47], they typically evaluate temporal generalization (forecasting future values at known locations) rather than spatial transfer. Time series regression with spatial transfer is substantially more challenging because models must simultaneously (1)

capture temporal dependencies and seasonal patterns, (2) learn representations that transfer across spatial domains with different temporal dynamics, and (3) handle regime shifts where the same temporal patterns may have different meanings in different locations (e.g., temperature fluctuations in tropical vs. polar ecosystems).

Absence of spatial transfer evaluation: No existing benchmark to our knowledge systematically evaluates spatial generalization i.e., the ability to transfer models to geographically distinct locations with different environmental conditions, ecosystem properties, or climatic regimes. This is a fundamental challenge in Earth system sciences [4, 35], ecology [19], agriculture [18], and public health [39], where observations are spatially sparse and expensive to collect, yet predictions are needed globally.

Need for scientific domain benchmarks: Scientific applications offer natural testbeds for spatial transfer learning: they feature genuine spatial heterogeneity (not artificial), provide interpretable feature spaces grounded in physical processes, and have clear societal impact. Yet they remain disconnected from the ML benchmarking ecosystem [19, 46]. Bridging this gap could accelerate both methodological innovation in transfer learning and scientific discovery in domain applications.

CarbonBench addresses these gaps by providing the first benchmark for spatial transfer learning in time series regression, grounded in a scientifically important application with real-world impact.

C Eddy Covariance Sites

Figure 7 shows the geographic distribution of all 567 sites included in CarbonBench, colored by Köppen climate classification. The spatial heterogeneity and concentration in North America and Europe motivates our dual stratification strategy. Figure 8 provides an example time series from site US-Ivo, illustrating the seasonal patterns in carbon fluxes and the quality flag annotations used in our training protocol.



Figure 7: Geographic distribution of 567 eddy covariance sites in CarbonBench, colored by Köppen climate classification.

D Training Protocol Details

D.1 Loss Function

To guide neural network training, we employ a composite loss function that has been shown to improve carbon flux prediction

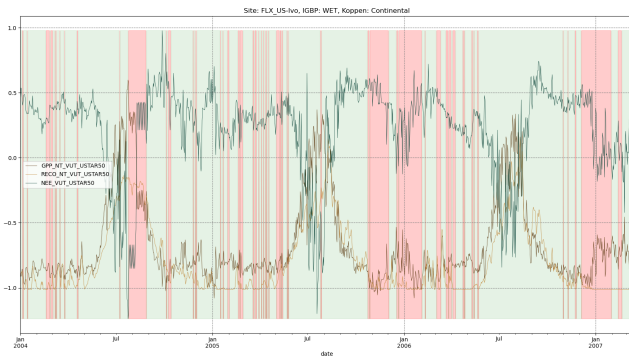


Figure 8: Example time series from FLUXNET site US-Ivo showing GPP, RECO, and NEE. Green regions indicate high-quality observations ($QC \geq 0.75$); red regions show lower-quality data ($QC < 0.75$).

in prior work [37]. This loss incorporates data quality weighting, class balancing, and physical consistency constraints:

$$\mathcal{L} = \text{MSE} \cdot w_{qc} \cdot w_{igbp} \cdot w_{koppfen} + \alpha \cdot \mathcal{L}_{flux}, \quad \alpha = 0.1$$

The loss components are defined as follows:

- **Quality weighting (w_{qc}):** Eddy covariance targets vary in reliability due to gap-filling and filtering procedures. We weight samples by their continuous quality flag $NEE_VUT_USTAR50_QC$ (ranging from 0 to 1), enabling partial utilization of lower-quality observations instead of binary exclusion.
- **Class balance weights (w_{igbp} , $w_{koppfen}$):** Flux tower coverage is highly uneven across land cover and climate classes (Table 1). We apply inverse-frequency weighting to increase loss contributions from underrepresented ecosystem and climate types.
- **Flux balance constraint (\mathcal{L}_{flux}):** To enforce physical consistency between targets, we penalize violations of the carbon balance relationship $NEE = RECO - GPP$.

For tree-based methods, we incorporate analogous sample weighting and class balancing through instance weights, ensuring that performance differences reflect architectural capabilities rather than preprocessing disparities.

D.2 Hyperparameter Optimization

We perform hyperparameter grid search for each architecture using 5-fold cross-validation stratified by Köppen climate class. Optimal configurations are then fixed and each model is trained with 10 different random seeds. Final predictions are obtained by averaging across seeds, reducing variance from stochastic initialization and mitigating spurious performance gains from favorable random seeds. Table 3 reports the selected hyperparameters for all models.

E Hyperparameter Configuration

All models were trained using cross-validation to select optimal hyperparameters. The best configurations for each model and data split are reported below.

E.1 Tree-Based Models

E.1.1 XGBoost.

- `colsample_bynode`: 1
- `learning_rate`: 0.05
- `max_depth`: 10
- `num_parallel_tree`: 1
- `objective`: `reg:squarederror`
- `tree_method`: `hist`
- `min_child_weight`: 5

E.1.2 LightGBM.

- `learning_rate`: 0.05
- `max_depth`: 10
- `min_child_weight`: 5
- `n_estimators`: 1000

E.2 Neural Network Models

Hyperparameter ranges:

- Hidden dimension: {64, 128, 256, 512}
- Dropout: {0.1, 0.2, 0.3, 0.4}
- Learning rate: {0.0001, 0.0005, 0.001, 0.005}
- Number of layers: {1, 2, 3}
- Transformer heads: {2, 4, 8}
- TAM-RL latent dimension: {16, 32, 64, 128}

All neural networks were trained with early stopping (`patience=20`) and the Adam optimizer. Training was conducted on NVIDIA A100 GPUs for 100 epochs maximum.

Table 3: Best hyperparameters for neural network models across different data splits. CV R² and RMSE represent average performance across validation folds.

Model	Split	Hidden	Dropout	LR	Layers	Other	CV R ²	CV RMSE
MLP	IGBP	128	0.2	0.0005	–	–	0.493	–
MLP	Köppen	256	0.3	0.0005	–	–	0.509	–
LSTM	IGBP	256	0.3	0.001	1	–	0.370	1.783
LSTM	Köppen	128	0.3	0.001	1	–	0.369	1.775
CT-LSTM	IGBP	128	0.2	0.0005	1	–	0.401	1.713
CT-LSTM	Köppen	256	0.3	0.0005	2	–	0.398	1.732
GRU	IGBP	128	0.3	0.0005	1	–	0.362	1.783
GRU	Köppen	256	0.2	0.0005	2	–	0.362	1.787
CT-GRU	IGBP	128	0.3	0.0005	1	–	0.399	1.709
CT-GRU	Köppen	128	0.3	0.0005	1	–	0.395	1.709
Transformer	IGBP	128	0.2	0.0005	2	nhead=4	0.387	1.729
Transformer	Köppen	128	0.2	0.0005	2	nhead=4	0.383	1.757
Patch-Transformer	IGBP	128	0.2	0.0005	2	nhead=4	0.329	1.832
Patch-Transformer	Köppen	128	0.2	0.0005	2	nhead=4	0.337	1.822
TAM-RL	IGBP	128	0.2	0.0001	2	latent=64	0.398	1.710
TAM-RL	Köppen	128	0.3	0.0001	1	latent=32	0.388	1.736